Red Sea tectonics unveil the largest known terrestrial ice stream: New constraints on Late Ordovician ice sheet dynamics

Mohamed Elhebiry
Western Michigan University https://orcid.org/0000-0002-0093-3404
Mohamed Sultan (mohamed.sultan@wmich.edu)
Western Michigan University
Abotalib Abotalib
Western Michigan University
Alan Kehew
Western Michigan University
Peter Voice
Western Michigan University
Ibrahim Abu El-Leil
Al-Azhar University

Article

Keywords: Mega-streamlined Landforms, Landscape Evolution, Paleo-climate Models, Ice Sheet Reconstructions, Morphological-based Constraints

Posted Date: July 6th, 2021

DOI: https://doi.org/10.21203/rs.3.rs-639303/v1

Red Sea tectonics unveil the largest known terrestrial ice stream: New constraints on Late Ordovician ice sheet dynamics

Authors

Mohamed S. Elhebiry[1,2], Mohamed Sultan[1*], Abotalib Z. Abotalib[1,3], Alan E. Kehew[1], Peter J. Voice[1], Ibrahim Abu El-Leil[2]

Affiliations

[1]Department of Geological and Environmental Sciences, Western Michigan University, Michigan, USA.

[2]Geology Department, Al-Azhar University, Cairo, Egypt.

[3]Geology Department, National Authority for Remote Sensing and Space Sciences, Cairo, Egypt.

Abstract

Mega-streamlined landforms on Earth and Mars have been attributed to aeolian, glaciogenic, fluvial, and tectonic processes. Identifying the forces that shaped these landforms is paramount for understanding landscape evolution and constraining paleo-climate models and ice sheet reconstructions. In Arabia, east-northeast, kilometer-scale streamlined landforms were interpreted to have been formed by Quaternary aeolian erosion. We provide field and satellite-based evidence for a Late Ordovician glacial origin for these streamlined landforms, which were exhumed during the Red Sea–related uplift. Then we use Late Ordovician paleo-topographic data to reconstruct the Late Ordovician ice sheet using identified and previously reported glacial deposits and landforms. Our reconstruction suggests these glacial features are part of a major, topographically controlled, marine-terminating ice stream, twice the length of the largest known

terrestrial ice streams. Our results support models that advocate for a single, major, and highly dynamic ice sheet and provide new morphological-based constraints for Late Ordovician climate models.

Introduction

The Late Ordovician glaciation event remains one of the most enigmatic climatic events in the Earth's history. The ice sheet initiation, duration, and extent of glaciation are subjects of debate. Lifetime estimates for the Late Ordovician glaciation range from a short-lived (0.5–1 Ma) Hirnantian ice sheet[1,2] to a ~10 Ma event in which the Hirnantian represented the climax of a much longer glacial period[3,4] to a long-lived glaciation that was initiated in the Middle Ordovician (Darriwilian) age[5–7].

Two models were proposed for the distribution of the Ordovician ice sheet(s): (1) a single, major ice sheet over Gondwanaland extending across North Africa, Arabia, South Africa, and South America[5,8,9], or (2) small ice caps in South Africa and South America separated from the northern ice sheet in North Africa and Arabia[10,11]. Late Ordovician glacial deposits and landforms are well reported from North Africa, Arabia, southern Europe, South Africa, and South America[10–13]. However, their localized and dispersed nature[5] hindered proper reconstruction of the ice sheet extent and the development of a comprehensive understanding of the Late Ordovician glaciation and ocean dynamics.

The vast extent of the Late Ordovician ice sheet (LOIS), with its Cenozoic-style climatic cyclicity[14] and its voluminous continental ice accumulations exceeding those of the last glacial maximum[3] (LGM) suggest a highly dynamic ice sheet with significant outlet glaciers and ice streams. However, the reported Late Ordovician ice streams[15] are confined to the Saharan

(western) part of the LOIS (Fig. 1A) and are limited in number compared to those reported from recent analogue ice sheets (e.g., the 117 ice streams in the Laurentide Ice Sheet[16]).

Ice streams—focused, fast-flowing ice conduits—are the "arteries" of ice sheets from which most (up to 90%) of the ice mass is discharged[17–19]. Identifying the position, extent, and length of paleo ice streams and the factors controlling their distribution is fundamental for reconstructing paleo ice sheets and delineating their geometries, intensity, and dynamics. Fortunately, paleo ice streams left behind clues (mega-streamlined morphologies) that were preserved for hundreds of millions of years on Earth[17] and apparently on other planets as well. Nevertheless, not all mega-streamlined landforms are glacial in origin[18,20]; multiple erosional processes such as aeolian and fluvial processes[21,22] or tectonic and magmatic activities[23] could have played a role in their formation.

Despite the early discoveries of the Late Ordovician glacial deposits in Arabia[24,25], no ice streams have been identified. Recently, Late Ordovician glacial deposits and exhumed subglacial mega-lineations (MLs) and landforms were reported from southeast Egypt over the Neoproterozoic basement rocks of the Arabian Nubian Shield[12]. On the other side of the Red Sea, and along the postulated extension of the newly reported glacial MLs, similar east-northeast–trending streamlined ridges were recognized in northwest Arabia over the Neoproterozoic basement of the Arabian Nubian Shield and the Cambro-Ordovician Saq Sandstone and were widely interpreted as mega-yardangs[26–28].

In this study, we provide evidence for a Late Ordovician glacial origin for the mega-streamlined landforms in Arabia. We then overlay these landforms together with previously reported glacial deposits and landforms on a Late Ordovician paleo-geomorphological reconstruction to identify the position and geometry of the largest known terrestrial ice stream, hereafter referred to as the

Late Ordovician Arabian Ice Stream (AIS). We show that our findings favor the single major LOIS model. Finally, we explain how our results could be used to constrain Late Ordovician climate models.

Geological Evolution

Four main lithologic packages (Neoproterozoic basement complex, Paleozoic sedimentary succession, Cenozoic Harrat basalts, and Quaternary An Nafud dunes; Fig. 1C) cover the study area. The Neoproterozoic basement complex was formed by protractive accretions during an extensive, prolonged (~300 My), convergent tectonic event forming the Arabian Nubian Shield[29]. The elevated land of the newly formed orogenic belt triggered intensive continental weathering and peneplanation processes, which resulted in thick clastic sedimentary successions of the Cambrian Siq Sandstone, the Cambro-Ordovician Saq Sandstone, and the Ordovician Qasim Formation[30,31] (Fig. 1). Northwest Arabia was then uplifted and the depositional processes were interrupted during the Middle to Late Ordovician in response to far-field effects of the Taconic orogeny, which incised valleys and canyons (paleo-valleys) within the Qasim Formation and exposed the underlying Saq Sandstone and basement complex[32]. Following the Taconic orogeny, the LOIS extended across North Gondwana, including the study area[12,25], and eroded and polished the exposures of the Neoproterozoic basement and the Saq sandstone, forming subglacial streamlined landforms, tunnel valleys and filled the paleo-valleys and canyons. The ice sheet retreated, sea levels rose, and Early Silurian shale was deposited over glacial sequences; together, they formed a glaciogenic petroleum system[15,33]. The Gondwana continent witnessed a second, longer (>70 My), Permo-Carboniferous glacial event, that was reported in southern, but not northern Arabia[12]. The south pole migrated in a southwest direction across Gondwana from northwest Africa in the Late Ordovician to central Antarctica during the Permo-

Carboniferous[9,34]. While the Gondwana continent was on the move, northwest Arabia was stationed during the Paleozoic and Mesozoic Eras in a near-shore location (i.e., coastal plains to continental shelf) where thick, shallow-to-slightly-deep marine clastic deposits were laid down over the Late Ordovician glacial deposits and landforms. Paleozoic rocks are exposed today in an arcuate belt around the margin of the Neoproterozoic basement[32] and can be divided into: (1) pre-glacial deposits comprising Cambrian to Ordovician Siq and Saq Sandstones and Qasim Formation; (2) glacial deposits (Zarqah and Sarah Formations); and (3) post-glacial Paleozoic deposits. The Late Ordovician glacial deposits and landforms were buried underneath the thick Paleozoic and Mesozoic post-glacial deposits until the onset of Red Sea–related uplifting in the Cenozoic, when the shoulders of the Red Sea rift were elevated and the crystalline basement and the overlying thick sedimentary successions including the glacial deposits were exposed[35]. Red Sea rifting was accompanied by emplacement of asymmetric flood basalts (Harrat) along the eastern flank of the rift starting some 30 Ma and extending into the Holocene period[36,37]. During the Pleistocene, the climate of northwest Arabia alternated between dry and wet periods[38], where wind erosion prevailed during the dry periods forming the great An Nafud dunes, and lake deposits were laid down within interdune depressions during the wet periods[39]. The prolonged geological evolution of the rock exposures in northwest Arabia suggests a complex landscape evolution, and thus interpretation of the formation mechanisms of different landforms must be considered with caution and should take the geological evolution of the area into account.

Results and Discussion

MLs shape and distribution

Landsat 8 multispectral images, together with Advanced Land Observing Satellite (ALOS) Phased Array L-band Synthetic Aperture Radar (PALSAR) radar and digital elevation model

(DEM) (SRTM 30 m and ALOS 12.5 m) data were utilized to map the streamlined MLs over the Neoproterozoic basement and the Saq Sandstone in northwest Arabia (Figs. 2A and B). The PALSAR data, with its deep penetration capabilities (up to 2 m), and sensitivity to roughness[40] was particularly useful in mapping the MLs in areas proximal to dunes. MLs were found to extend over the Neoproterozoic basement and the pre-glacial Saq Sandstone along an east-northeast trend for ~400 km. The MLs over the Neoproterozoic basement display the following morphometric parameters: subparallel valleys (mega-grooves; negative topography) separated by parallel ridges extending for tens of kilometers in length, a few hundreds of meters in width, and tens of meters in depth (Figs. 2C and E), and length-to-width ratios ranging from 50:1 to >100:1. Some of the megagrooves show a parabolic U-shaped valley morphology with hanging valleys cutting the side walls (Figs. 2D and F). The MLs extend over crystalline basement rocks units of varying compositions, textures, and modes of emplacement and deposition (e.g. massive, foliated, intrusions, volcanics, and metasediments41; Fig. 2).The MLs over the Saq Sandstone found to the north and east of the basement MLs have similar orientation trends, but display different morphometric parameters (length: 1–6 km; width: few hundred meters and up to 1 km; height: 5–50 m; length/width ratio: ~10:1; Fig. 1C). The consistency of MLs trends, but not their morphometric parameters, over both the crystalline rocks and Paleozoic sandstones, indicates bedrock control on mega-lineated landform distribution. Similar bedrock controls on morphometric parameters of subglacial landforms were documented in recent glacial landforms[18].

Origin of the MLs

The east-northeast trends of the streamlined MLs are different from the reported northerly and northwesterly structural trends[36] in the area (Fig. 1C), which rules out a possible tectonic origin

for these MLs. This suggestion is further supported by the absence of extensive deformation (brittle or ductile) along the east-northeast trend in the mapped area on both sides of the Red Sea[12,36,41] (Fig. 1). Also, the fact that the mapped MLs maintain consistent trends for hundreds of kms over crystalline rocks of varying compositions, textures, and modes of emplacement and deposition argues against structural control of the MLs orientation by specific internal features of rock units (e.g. bedding orientations, fracture patterns, foliations, or other linear fabrics).

Earlier studies which considered these streamlined landforms as mega-yardangs[26–28] were biased by the presence of transverse barchan dunes along and orthogonal to the extension of the MLs in the northern part of the study area (Fig. 3A). Here, we provide evidence in support of a Late Ordovician glacial origin of these streamlined landforms and argue against an aeolian origin. First, the streamlined beds are sub parallel to the wind directions (southwest to northeast; inferred from the barchan dunes orientation in An Nafud desert) in the northern part of the study area[27,28] (Fig. 3A), but not in the central and southern sections, where the MLs are at high angles to the wind direction (from northwest to southeast; inferred from the longitudinal dune trend; Fig. 3B). Second, the mapped MLs were identified over the preglacial rock units (Neoproterozoic basement and the Cambro-Ordovician Saq Sandstone) but not over glacial or post-glacial deposits (Figs. 1C, 3C and 3D). Third, the morphometric parameters (elongation ratios 10 to >100) of the MLs are similar to those reported for subglacial MLs over hard beds[18] but different from the ratios reported for yardangs (3.5 to 5)[28,42]. Also, their morphology over the basement (parallel U-shaped valleys interpreted here as glacial mega-grooves; Figs. 2C, D, E and F) is different from the morphology of yardangs (parallel ridges), a difference that was realized by Brown et al.[26] and led them to classify them as trough yardangs instead of normal yardangs. Fourth, yardangs are formed over soft beds and are largely composed of fluvial/lacustrine

159 sediments[28,43]. To the best of our knowledge, the only exception comes from a questionable
160 remote sensing–based study in which mega-yardangs were reported over crystalline basement in
161 Namibia[43,44]. Fifth, the mapped MLs are parallel to the reported glacial striation and tunnel
162 valley trends[25] and align with the recently reported Late Ordovician MLs in southeastern Egypt[12]
163 (Fig. 1B). Sixth, numerous well documented, preserved, small-scale, glacial features (e.g.
164 striated and grooved glacial surfaces, roche moutonnées, and tunnel valleys) are found within the
165 area where the MLs are mapped[25,45,46]. The above-mentioned observations are consistent with a
166 glacial origin for the MLS and the presence of Neoproterozoic basement cobbles and boulders
167 (up to 1 m in diameter) within the lower tillite layer of the glacial deposits of Sarah Formation in
168 the eastern part of the shield[25,46] is consistent with the LOIS being in direct contact with the
169 crystalline basement.

170 On the other side of the Red Sea, in the southern part of the Eastern Desert of Egypt (SED),
171 similar MLs were observed and reported by our research team[12] (Fig. 1B). The MLs of the SED
172 extend for over 200 km in an east-northeast-direction, a direction orthogonal to the reported
173 north to south wind trajectories[47]. The streamlined landforms display morphometric parameters
174 (megagrooves: length 10s km; width 100s m; and depth 10s m) and field relations (observed over
175 Neoproterozoic crystalline basement, but not over post-Ordovician deposits) similar to those
176 observed in northern Arabia[12].

177 Several outcrops of glacial deposits (i.e., diamictites) and features (i.e., glacial polished
178 pavement) were observed by our team in the SED, in areas where MLs were mapped. Those
179 include massive, unsorted, boulder rich (up to 1 meter in diameter) and matrix-supported
180 diamictites that unconformably overly the crystalline basement (e.g. Wadi El-Naam, and Korbiai
181 areas; Figs. 4A and B). Most of those deposits were eroded during the Red Sea-related uplift, but

a few were preserved in paleo-topographic depressions within basement rocks (e.g. Betan area: Fig. 4C). Glacial polished pavements over the Neoproterozoic granitic intrusions were observed in Jebel Hagar Zarqa at the Gerf area, SED (Figs. 4D and E). Again, these observations from the SED and those reported from northern Arabia are consistent with the LOIS being in direct contact with the crystalline basement of the Arabian-Nubian Shield.

The pre-Gondwana breakup (pre-Jurassic) morphological features and landforms were thought to be less likely to be preserved and exposed in Afro-Arabia especially in the tectonically active areas as the Red Sea rift[48,49]. Our observations, however, indicate that the Late Ordovician MLs were protected by the overlying thick Paleozoic clastic sedimentary cover until the Cenozoic when the Red Sea–related uplift began. The uplift led to exhumation of the basement complex and the overlying sedimentary sequences (5–15 km) and landforms along the Red Sea Hills and shoulders[35,50,51]. No MLs were recognized over the rugged basement outcrops near the rift shoulders on both sides of the Red Sea, possibly due to the high exhumation rate. A few tens of kilometers away on both sides of the Red Sea, the Late Ordovician landforms were exposed on gently dipping Neoproterozoic peneplains (Figs. 1B and 1C), but remained buried underneath the overlying Paleozoic clastic successions a few hundred kilometers further away (Fig. 1)[12]. The above-mentioned observations support a Late Ordovician glacial erosional origin for the streamlined features, which were later exhumed by the Red Sea–related uplift. Many of the streamlined features over the Saq Sandstone in the northern part of the study area were polished and widened by wind erosion.

Late Ordovician Arabian Ice Stream (AIS)

The identification of Paleozoic ice streams has been almost exclusively based on the presence of long subglacial bed forms (elongation ratio 10–100)[20]. The presence of long bed forms is

indicative of fast ice flow[52,53], yet they do not fully portray the extent and type of the ice stream in question. This is especially true for Paleozoic ice streams, where many of the streamlined beds may have not been completely preserved or might not have been exposed for mapping. To address this issue, we first reconstruct the distribution of the mapped glacial MLs and the reported glacial deposits in the Late Ordovician using a paleo-geomorphologic (paleo-DEM) dataset (445 Ma; resolution: 1° × 1°; Supplementary materials) [54], then identify the factors (e.g., topographic focusing and calving margins) that control the extension and the distribution of ice streams in recent analogues[16,55,56], and finally use these factors to map ice streams and their projected extension in areas where the streamlined morphologies are not exposed.

Our analysis revealed the presence and distribution of an impressive ice stream extending over a distance of 3000 km from southeastern Egypt into northern and central Saudi Arabia across the Arabian Peninsula and terminating in the paleo-Tethys (Fig. 5A). The proposed distribution of the AIS is supported by the following observations. First, the initiation of the ice stream in southeast Egypt is based on the presence of a high topographic obstacle (>2000 m)[54,57,58] represented by the orogenic belt of the Arabian Nubian Shield, which apparently impeded the west-to-east advancement of the LOIS south of the identified ice stream and focused ice flow at the ice stream location (Fig. 5A), a phenomenon known as topographic focusing (the most influential control on recent ice streams)[16,17]. Our interpretation of the Arabian Nubian Shield as a topographic barrier blocking the advancement of the ice sheet south of the AIS is further supported by the presence of Late Ordovician glacial deposits in Eritrea and Ethiopia (west; Fig. 1A)[59,60] and their absence in southern and central Arabia (east; Figs. 1C and 3). Second, subglacial meltwater routing along the proposed east-northeast–trending AIS is supported by the presence of tunnel valleys trending in similar directions[25] and by the presence of the glacial gold

placer deposits that were formed by the action of subglacial pressurized meltwater in southern Egypt[12]. Third, the proposed extent of the ice sheet hundreds of kilometers over the continental shelf in the reconstructed Late Ordovician geographical maps (Fig. 5A) is supported by the discovery of glaciomarine and iceberg deposits to the east of the ice stream (present-day location in western Iran; Fig. 1)[61] that indicate the presence of a calving margin at the AIS terminal. The paleo-slopes measurements reported from the incisions in the Dargaz Formation in western Iran[61], are consistent with the orientation of the tunnel valleys[25] and the advocated AIS in Saudi Arabia. Additional evidence in support of the advocated distribution of the AIS comes from the Hirnantian graptolite assemblages recovered from the Dargaz Formation in western Iran, where high abundance of *Normalograptus ajjeri* and rare occurrence of *Normalograptus persculptus* were reported[61], a pattern that is diagnostic of graptolite associations from North African and Arabian Ordovician rocks[61,62].

The above-mentioned lines of evidence, together with the highly attenuated landforms (elongation ratio 10 to >100; Figs. 2A and B), suggest that these glacial features are a part of an extensive, topographically controlled, marine-terminating Late Ordovician ice stream (>2500 km in terrestrial extent and up to 500 km on the continental shelf). The identified AIS of the LOIS is more than twice the length of the longest Quaternary ice streams (Fig. 5B). The Quaternary Laurentide Ice Sheet has the longest known ice streams, extending for ~1000 to 1300 km (e.g., M'Clure Strait and Hudson Straits, Canada). The presence of MLs and subglacial landforms over crystalline hard beds, which is the case with the AIS, has been cited as evidence for long-lived ice streams[18].

Ice sheet reconstruction

Continental ice sheets are significant components of paleoclimatic models. In deep-time climate modeling, the surface air temperatures, continental ice volume, atmospheric circulation, ice-ocean interactions, and CO_2 threshold values for glacial onset are significantly affected by the change in the ice sheet extent and ice surface elevations that are largely controlled by ice stream geometry and distribution[5,63,64]. Ordovician climate models showed that the ice stream distribution and topographic elevations can exert significant controls on ice volume estimates, where the addition of ice streams reduced the estimated ice volume by some 40%[5]. A northern ice sheet model covering north Gondwana (Africa-Arabia) with small isolated ice caps in southern Africa and South America was proposed by Le Heron and Dowdeswell[10] who based their suggestion on the limited sedimentary fluxes that were estimated from the previously identified ice streams across the Saharan part of the ice sheet only. The stability of mid-latitude ice caps was challenged by recently published climatic models for the Late Ordovician period that called on a single major ice sheet covering Gondwanaland from the pole to tropics and extending from North Africa–Arabia to South Africa and South America[5,9,63]. Our findings of a major AIS supports the single major LOIS models and is inconsistent with others that call on a smaller ice sheet extent in northern Gondwana. We cite two lines of evidence. First, the earlier estimates for the ice volume of the smaller ice sheet was based on the cumulative ice stream fluxes from the Saharan ice streams only[10,65]. Adding a new major long-lived ice stream, namely the AIS and possibly others yet to be discovered, will significantly increase the estimates of ice stream fluxes and ice sheet volumes. Second, a general correlation has been recognized between the volume of ice sheets and the length of their ice streams; the larger the volume of ice, the longer the length of the ice streams[16,55,56]. Thus, the large extension of the AIS—more than twice

the length of the longest of the Quaternary ice sheets—supports an extensive Late Ordovician ice sheet compared to the Quaternary ice sheets.

The eastern Gondwana peripheral glacial and glacio-marine occurrences from the Late Ordovician ice sheet in western Iran and southern Turkey were thought to have originated from isolated and elevated ice caps over the Arabian Nubian Shield[61,66] or from an ice lobe connected with the main LOIS[67]. Our reconstruction indicates a similar origin for the western Iran glacio-marine deposits; it originated from the main ice sheet and was transported by the AIS (Fig. 5). The reconstruction also confirms the connection between the Saharan and Arabian part of the Late Ordovician ice sheet given juxtaposition of the MLs in Africa and Arabia and the alignment of their trends.

Our Late Ordovician ice sheet reconstruction suggests extensive mid-latitude (~ 40°) calving margins at the front of the AIS in the continental shelf of northeast Gondwana (Fig. 5A). This suggestion is consistent with the newly reported Late Ordovician iceberg deposits from the subtropical shelf of Baltica sourced from the Northern African–Arabian margin[8]. Moreover, the presence of the AIS calving margins in the eastern margin of Gondwana resolves the dilemma raised from the fact that the isopach map of the icebergs in Baltica shelf indicates southeast sourced icebergs that were driven northwestward and adds a line of evidence in support of the suggested cold water linkage between the Arabian margins and Baltica as a "source to sink" route for the Late Ordovician eastern margin icebergs[8].

Implications

Most of the subglacial landforms of the Paleozoic ice sheets are not preserved or are unexposed. The MLs, although indicative of the presence of ice streams, do not on their own provide a comprehensive understanding of the ice sheet dynamics and extent[65]. The Late Ordovician

295 reconstructions for the identified landforms and striation trends that we developed and their
296 spatial correlations with paleo-topographic datasets address—at least in part—these apparent
297 shortcomings. It allows the identification of topographic controls for the investigated ice streams
298 and provides a more realistic distribution and extent for the Late Ordovician ice streams. Our
299 findings potentially provide additional constraints and refinements for a wide range of Late
300 Ordovician climate models; the presence of extensive ice streams, similar to the one described
301 here (the AIS) provides evidence for a highly dynamic LOIS. The major calving margins
302 identified in eastern Gondwana in the front of the AIS confirm the recently suggested Late
303 Ordovician counter-clockwise ocean circulation northwestward from Arabia (source) to Baltica[8]
304 as a new constraint for Late Ordovician climate models.

305 Our findings show that subglacial AIS-related MLs were misclassified as mega-yardangs and
306 raise the question of whether similar misinterpretations could have been made in other parts of
307 the arid and hyper-arid world, and possibly more so on Mars, where MLs are much less likely to
308 be obscured or modulated by tectonic activities. Ice streams could have carved mega-lineated
309 flutes in the Martian outflow channels during earlier warmer climatic periods on Mars[68,69];
310 discoveries of liquid water beneath the Martian south polar layered deposits[70] suggest recent
311 basal melting of Martian ice sheets[71]. The long glacial cycles due to the Earth's high amplitude
312 obliquity modulation in the Ordovician ($>10^6$ yr)[14] that compared well with the Martian
313 amplitude modulation[72,73] and the presence of the large polar landmass of Gondwana raises the
314 suggestion that the AIS-related landforms could potentially present a better analogue to Martian
315 glacial landforms than Quaternary landforms[74,75].

316 The identified AIS could have significant implications for hydrocarbon exploration. Oil and gas
317 are being produced from the Late Ordovician ice stream deposits in the Saharan part of the LOIS

(Libya and Algeria)[15,33]. Given the large size of the identified AIS and the voluminous sedimentary flux hosted within it, significant untapped hydrocarbon reserves could be residing within the AIS.

Methods

A threefold methodology was adopted. First, we mapped the MLs and extracted their morphometric parameters (length/width ratio) using the following remote sensing products: (1) multispectral Landsat 8 images (bands 7, 5, and 3) to map the large-scale morphological trends (ridges/valleys) over the basement and Saq Sandstone; (2) Advanced Land Observing Satellite (ALOS) Phased Array L-band Synthetic Aperture Radar (PALSAR) data downloaded from the global PALSAR-2/PALSAR mosaic (25 m spatial resolution) to validate the Landsat-based MLs distribution, especially in areas where the mega-ridges (rough surface: high backscatter, bright) interleaved with valleys partially filled with fine-grained sand and silt (low backscatter, dark) (Fig. 3C); (3) high-resolution (spatial resolution: up to 30 cm) multispectral base map imagery available on the Arc GIS Online base map and Google Earth to map the smaller linear features over the Saq sandstone and to obtain high resolution topographic profiles (Figs. 2C, D, E and F), the ALOS PALSAR DEM (spatial resolution: 12.5 m) to delineate and visualize (in 3D) the mega-ridges and to map the distribution of dunes (linear and barchan) and infer wind directions (Fig. 3B), and Shuttle Radar Topography Mission (SRTM) DEM mosaics (spatial resolution: 30 m) to enable 3D visualization in areas where the ALOS PALSAR DEM is not available (Fig. 3A).

Second, we generated a GIS platform to host all relevant data in a unified geographic projection (datum WGS-84: using ESRI ArcMap V. 10.6.1), integrate observations extracted from these datasets, and conduct spatial correlations and analyses to investigate the origin of the MLs. The

GIS encompasses the following spatial datasets: (1) published data including geologic maps (scale: 1:1250,000 and 1:1000,000) and the associated field observations and explanatory notes[45,46,76–78], (2) mosaics of the remote sensing data sets and the interpreted east-northeast MLs features, (3) structural trends extracted from the 1:250,000 quadrangle maps, and (4) reported Late Ordovician glacial deposits, landforms, striation trends, and ice streams.

Third, we used the GPlates software to generate a Late Ordovician (450 Ma) reconstruction that displays the distribution of the mapped MLs in northwest Arabia and southeast Egypt, as well as the previously reported striation trends, tunnel valleys, subglacial, and glaciomarine deposits in the Arabian part of the ice sheet. All of these elements were plotted onto a paleo-topographic map initiated using Paleo-Digital Elevation Model data sets (Paleo-DEM, 1° x 1° resolution)[54].

References

1. Sutcliffe, O. E., Dowdeswell, J. A., Whittington, R. J., Theron, J. N. & Craig, J. Calibrating the Late Ordovician glaciation and mass extinction by the eccentricity cycles of Earth's orbit. *Geology* **28**, 967–970 (2000).

2. Brenchley, P. J. *et al.* Bathymetric and isotopic evidence for the short-lived Late Ordovician glaciation in a greenhouse period. *Geology* **22**, 295–2598 (1994).

3. Finnegan, S. *et al.* The magnitude and duration of late Ordovician-early Silurian glaciation. *Science (80-.).* **331**, 903–906 (2011).

4. Saltzman, M. R. & Young, S. A. Long-lived glaciation in the Late Ordovician? Isotopic and sequence-stratigraphic evidence from western Laurentia. *Geology* **33**, 109–112 (2005).

5. Pohl, A. *et al.* Glacial onset predated Late Ordovician climate cooling. *Paleoceanography* **31**, 800–821 (2016).

6. Pohl, A. & Austermann, J. A sea-level fingerprint of the Late Ordovician ice-sheet collapse. *Geology* **46**, 595–598 (2018).

7. Trotter, J. A., Williams, I. S., Barnes, C. R., Lécuyer, C. & Nicoll, R. S. Did cooling oceans trigger Ordovician biodiversification? Evidence from conodont thermometry. *Science (80-.).* **321**, 550–554 (2008).

8. Porębski, S. J. *et al.* Hirnantian icebergs in the subtropical shelf of Baltica: Evidence from sedimentology and detrital zircon provenance. *Geology* **47**, 284–288 (2019).

9. Torsvik, T. H. & Cocks, L. R. M. Gondwana from top to base in space and time. *Gondwana Res.* **24**, 999–1030 (2013).

10. Le Heron, D. P. & Dowdeswell, J. A. Calculating ice volumes and ice flux to constrain the dimensions of a 440 Ma North African ice sheet. *J. Geol. Soc. London.* **166**, 277–281 (2009).

11. Ghienne, J.-F., Le Heron, D. P., Moreau, J., Denis, M. & Deynoux, M. The Late Ordovician Glacial Sedimentary System of the North Gondwana Platform. *Glacial Sediment. Process. Prod.* **39**, 295–319 (2007).

12. Elhebiry, M. S. *et al.* Paleozoic glaciation in NE Africa: field and remote sensing-based evidence from the South Eastern Desert of Egypt. *Int. Geol. Rev.* **62**, 1187–1204 (2020).

13. Díaz-Martínez, E. & Grahn, Y. Early Silurian glaciation along the western margin of Gondwana (Peru, Bolivia and northern Argentina): Palaeogeographic and geodynamic

setting. *Palaeogeogr. Palaeoclimatol. Palaeoecol.* **245**, 62–81 (2007).

14. Ghienne, J. F. *et al.* A Cenozoic-style scenario for the end-Ordovician glaciation. *Nat. Commun.* **5**, 1–9 (2014).

15. Le Heron, D. P., Craig, J. & Etienne, J. L. Ancient glaciations and hydrocarbon accumulations in North Africa and the Middle East. *Earth-Science Rev.* **93**, 47–76 (2009).

16. Margold, M., Stokes, C. R. & Clark, C. D. Ice streams in the Laurentide Ice Sheet: Identification, characteristics and comparison to modern ice sheets. *Earth-Science Rev.* **143**, 117–146 (2015).

17. Stokes, C. R. & Clark, C. D. Palaeo-ice streams. *Quat. Sci. Rev.* **20**, 1437–1457 (2001).

18. Krabbendam, M., Eyles, N., Putkinen, N., Bradwell, T. & Arbelaez-moreno, L. Streamlined hard beds formed by palaeo-ice streams: A review. *Sediment. Geol.* **338**, 24–50 (2016).

19. Spagnolo, M. *et al.* Size, shape and spatial arrangement of mega-scale glacial lineations from a large and diverse dataset. *Earth Surf. Process. Landforms* **1448**, 1432–1448 (2014).

20. Moreau, J., Ghienne, J. F., Le Heron, D. P., Rubino, J. L. & Deynoux, M. 440 Ma ice stream in North Africa. *Geology* **33**, 753–756 (2005).

21. Russell, P. S. & Head, J. W. Elysium-Utopia flows as mega-lahars: A model of dike intrusion, cryosphere cracking, and water-sediment release. *J. Geophys. Res. E Planets* **108**, (2003).

22. Abotalib, A. Z., Sultan, M. & Elkadiri, R. Groundwater processes in Saharan Africa:

Implications for landscape evolution in arid environments. *Earth-Science Rev.* **156**, 108–136 (2016).

23. Ernst, R., Grosfils, E. & Mège, D. Giant dike swarms: Earth, Venus, and Mars. *Annu. Rev. Earth Planet. Sci.* **29**, 489–534 (2001).

24. McClure, H. A. Early paleozoic glaciation in Arabia. *Palaeogeogr. Palaeoclimatol. Palaeoecol.* **25**, 315–326 (1978).

25. Vaslet, D. Upper Ordovician glacial deposits in Saudi Arabia. *Episodes* **13**, 147–161 (1990).

26. Brown, G. F., Schmidt, D. L. & Huffman Jr, A. C. *Geology of the Arabian Peninsula, Shield Area of Western Saudi Arabia*. *U.S. Geological Survey Professional Paper* **560**-**A**, (USGS, 1989).

27. Vincent, P. & Kattan, F. Yardangs on the Cambro-Ordovivian Saq Sandstone, North-West Saudi Arabia. *Z. Geomorph. N. F.* **50**, 305–320 (2006).

28. Goudie, A. S. Mega-yardangs: A global analysis. *Geogr. Compass* **1**, 65–81 (2007).

29. Stern, R. J. ARC assembly and continental collision in the Neoproterozoic East African Orogen: Implications for the Consolidation of Gondwanaland. *Annu. Rev. Earth Planet. Sci.* **22**, 319–351 (1994).

30. Husseini, M. I. The Cambro-Ordovician Arabian and adjoining plates: a glacio-eustatic model. *J. Pet. Geol.* **13**, 267–288 (1990).

31. Konert, G., Afifi, A. M., Al-Hajri, S. A. & Droste, H. J. Paleozoic stratigraphy and hydrocarbon habitat of the Arabian plate. *GeoArabia* **6**, 407–442 (2001).

32. Laboun, A. A. Regional tectonic and megadepositional cycles of the Paleozoic of northwestern and central Saudi Arabia. *Arab. J. Geosci.* **6**, 971–984 (2013).

33. Huuse, M. *et al.* Glaciogenic reservoirs and hydrocarbon systems : an introduction. *Geol. Soc. London, Spec. Publ.* **368**, 1–28 (2012).

34. Scotese, C. R. & Barrett, S. F. Gondwana's movement over the South Pole during the Palaeozoic: evidence from lithological indicators of climate. *Geol. Soc. London, Mem.* **12**, 75–85 (1990).

35. Bosworth, W., Huchon, P. & McClay, K. The Red Sea and Gulf of Aden Basins. *J. African Earth Sci.* **43**, 334–378 (2005).

36. Stern, R. J. & Johnson, P. Continental lithosphere of the Arabian Plate: A geologic, petrologic, and geophysical synthesis. *Earth-Science Rev.* **101**, 29–67 (2010).

37. Camp, V. E., Roobol, M. J. & Hooper, P. R. The Arabian continental alkali basalt province: part III. Evolution of Harrat Kishb, Kingdom of Saudi Arabia. *Geol. Soc. Am. Bull.* **104**, 379–396 (1992).

38. Abotalib, A. Z. *et al.* Complexity of Saharan paleoclimate reconstruction and implications for modern human migration. *Earth Planet. Sci. Lett.* **508**, 74–84 (2019).

39. Rosenberg, T. M. *et al.* Middle and Late Pleistocene humid periods recorded in palaeolake deposits of the Nafud desert, Saudi Arabia. *Quat. Sci. Rev.* **70**, 109–123 (2013).

40. Xiong, S., Muller, J. P. & Li, G. The application of ALOS/PALSAR InSAR to measure subsurface penetration depths in deserts. *Remote Sens.* **9**, 1–19 (2017).

41. Brown, G. F., Layne, N., Goudarzi, G. H. & MacLean, W. H. *Geologic map of the*

northeastern Hijaz quadrangle, Kingdom of Saudi Arabia. *IMAP* (1963). doi:10.3133/i205A

42. Ghodsi, M. Morphometric characteristics of Yardangs in the Lut Desert, Iran. *Desert* **22**, 21–29 (2017).

43. Ding, Z., Zhao, J., Wang, J. & Lai, Z. Yardang on Earth and its implications to Mars: A review. *Geomorphology* **364**, (2020).

44. Goudie, A. S. & Viles, H. *Landscapes and Landforms of Namibia*. *World Geomorphological Landscapes* **28**, (Springer International Publishing, 2015).

45. Vaslet, D. *et al. Explanatory notes to the Geologic Map of the Tayma' Quadrangle, Sheet 27c, kingdom of Saudi Arabia*. (1994).

46. Janjou, D. *et al. Geologic map of the Tabuk Quadrangle, Sheet 28B, Kingdom of Saudi Arabia*. (1997).

47. Brookes, I. A. Geomorphic indicators of Holocene winds in Egypt ' s Western Desert. **56**, 155–166 (2003).

48. Partridge, T. C. & Maud, R. R. Geomorphic evolution of Southern Africa since the Mesozoic. *South. African J. Geol.* **90**, 179–208 (1987).

49. Burke, K. & Gunnell, Y. The african erosion surface: A continental-scale synthesis of geomorphology, tectonics, and environmental change over the past 180 million years. in *Geological Society of America* (eds. Burke, K. & Gunnell, Y.) **Memoir 201**, 1–66 (Geological Society of America, 2008).

50. Almalki, K. A., Betts, P. G. & Ailleres, L. The Red Sea – 50 years of geological and

geophysical research. *Earth-Science Rev.* **147**, 109–140 (2015).

51. Bojar, A. V., Fritz, H., Kargl, S. & Unzog, W. Phanerozoic tectonothermal history of the Arabian-Nubian shield in the Eastern Desert of Egypt: Evidence from fission track and paleostress data. *J. African Earth Sci.* **34**, 191–202 (2002).

52. Stokes, C. R. & Clark, C. D. Are long subglacial bedforms indicative of fast ice flow? *Boreas* **31**, 239–249 (2002).

53. King, E. C., Hindmarsh, R. C. A. & Stokes, C. R. Formation of mega-scale glacial lineations observed beneath a West Antarctic ice stream. *Nat. Geosci.* **2**, 585–588 (2009).

54. Scotese, C. R. & Wright, N. PALEOMAP Paleodigital Elevation Models (PaleoDEMS) for the Phanerozoic PALEOMAP Project. 1–26 (2018).

55. Stokes, C. R., Margold, M., Clark, C. D. & Tarasov, L. Ice stream activity scaled to ice sheet volume during Laurentide Ice Sheet deglaciation. *Nature* **530**, 322–326 (2016).

56. Winsborrow, M. C. M., Clark, C. D. & Stokes, C. R. What controls the location of ice streams? *Earth-Science Rev.* **103**, 45–59 (2010).

57. Pohl, A., Donnadieu, Y., Le Hir, G., Buoncristiani, J.-F. & Vennin, E. Effect of the Ordovician paleogeography on the (in) stability. *Clim. Past* **10**, 2053–2066 (2014).

58. Scotese, C. R. *PALEOMAP PaleoAtlas for GPlates and the PaleoData Plotter Program*. (2016). doi:10.13140/RG2.2.34367.00166

59. Lewin, A., Meinhold, G., Hinderer, M., Dawit, E. L. & Bussert, R. Provenance of sandstones in Ethiopia during Late Ordovician and Carboniferous – Permian Gondwana glaciations : Petrography and geochemistry of the Enticho Sandstone and the Edaga Arbi

Glacials. *Sediment. Geol.* **375**, 188–202 (2018).

60. Bussert, R. Exhumed erosional landforms of the Late Palaeozoic glaciation in northern Ethiopia: Indicators of ice-flow direction, palaeolandscape and regional ice dynamics. *Gondwana Res.* **18**, 356–369 (2010).

61. Ghavidel-syooki, M. *et al.* Stratigraphic evidence for the hirnantian (latest ordovician) glaciation in the zagros mountains, Iran. *Palaeogeogr. Palaeoclimatol. Palaeoecol.* **307**, 1–16 (2011).

62. Loydell, D. K. Graptolites from the upper ordovician and lower silurian of Jordan. *Spec. Pap. Palaeontol.* 1–66 (2007). doi:10.1111/j.1475-4983.2007.00712.x

63. Lowry, D. P., Poulsen, C. J., Horton, D. E., Torsvik, T. H. & Pollard, D. Thresholds for Paleozoic ice sheet initiation. *Geology* **42**, 627–630 (2014).

64. Quiquet, A., Dumas, C., Ritz, C., Peyaud, V. & Roche, D. M. The GRISLI ice sheet model (version 2.0): calibration and validation for multi-millennial changes of the Antarctic ice sheet. *Geosci. Model Dev.* **11**, 5003–5025 (2018).

65. Le Heron, D. P. & Craig, J. First-order reconstructions of a Late Ordovician Saharan ice sheet. *J. Geol. Soc. London.* **165**, 19–29 (2008).

66. Moix, P. *et al.* A new classification of the Turkish terranes and sutures and its implication for the paleotectonic history of the region. *Tectonophysics* **451**, 7–39 (2008).

67. Ghienne, J. F., Monod, O., Kozlu, H. & Dean, W. T. Cambrian-Ordovician depositional sequences in the Middle East: A perspective from Turkey. *Earth-Science Rev.* **101**, 101–146 (2010).

510 68. Lucchitta, B. K., Anderson, D. M. & Shoji, H. Did ice streams carve martian outflow
511 channels? *Nature* **290**, 759–763 (1981).

512 69. Pacifici, A., Komatsu, G. & Pondrelli, M. Geological evolution of Ares Vallis on Mars:
513 Formation by multiple events of catastrophic flooding, glacial and periglacial processes.
514 *Icarus* **202**, 60–77 (2009).

515 70. Orosei, R. *et al.* Radar evidence of subglacial liquid water on Mars. *Science (80-.).* **361**,
516 490–493 (2018).

517 71. Arnold, N. S., Conway, S. J., Butcher, F. E. G. & Balme, M. R. Modeled subglacial water
518 flow routing supports localized intrusive heating as a possible cause of basal melting of
519 Mars' south polar ice cap. *J. Geophys. Res. Planets* **124**, 2101–2116 (2019).

520 72. Ward, W. R. Large-scale variations in the obliquity of Mars. *Science (80-.).* **181**, 260–262
521 (1973).

522 73. Ward, W. R. & Rudy, D. J. Resonant obliquity of Mars? *Icarus* **94**, 160–164 (1991).

523 74. Lucchitta, B. K. Antarctic ice streams and outflow channels on Mars. *Geophys. Res. Lett.*
524 **28**, 403–406 (2001).

525 75. Banks, M. E. *et al.* An analysis of sinuous ridges in the southern Argyre Planitia, Mars
526 using HiRISE and CTX images and MOLA data. *J. Geophys. Res. E Planets* **114**, 1–19
527 (2009).

528 76. Ekren, E., Vaslet, D., Berthiaux, A., Le Strat, P. & Fourniguet, J. *Geologic Map of the*
529 *Ha'il Quadrangle, Sheet 27 E, Kingdom of Saudi Arabia*. (1987).

530 77. Manivit, J., Vaslet, D., Berthiaux, A., Le Strat, P. & Fourniguet, J. *Geologic map of the*

Buraydah Qudrangle, Sheet 26 G, Kingdom of Saudi Arabia. (1986).

78. Janjou, D. *et al. Geologic map of the Al Qalibah Quadrangle, Sheet 28 C, Kingdom of Saudi Arabia*. (1996).

Acknowledgments

We thank Dr. Daniel Le Heron from the University of Vienna for his valuable suggestions on an earlier version of the manuscript.

Funding

This research was supported by the Earth Sciences Remote Sensing (ESRS) facility, Western Michigan University and by the Egyptian Cultural Affairs and Missions Sector, Ministry of Higher Education (Plan 2015-2016).

Author contributions

M.S.E., M.S., A.E.K. and A.Z.A. conceived and conceptualized the study. M.S.E. and I.A. conducted the fieldwork. M.S.E. and M.S. processed the data and generated the model. MSE and M.S. wrote the Manuscript. A.E.K., A.Z.A, P.J.V. and I.A. contributed and reviewed the manuscript.

Materials & Correspondence

Correspondence and requests for materials should be addressed to M.S.E.

Competing interests

The authors declare no competing interests.

Figures

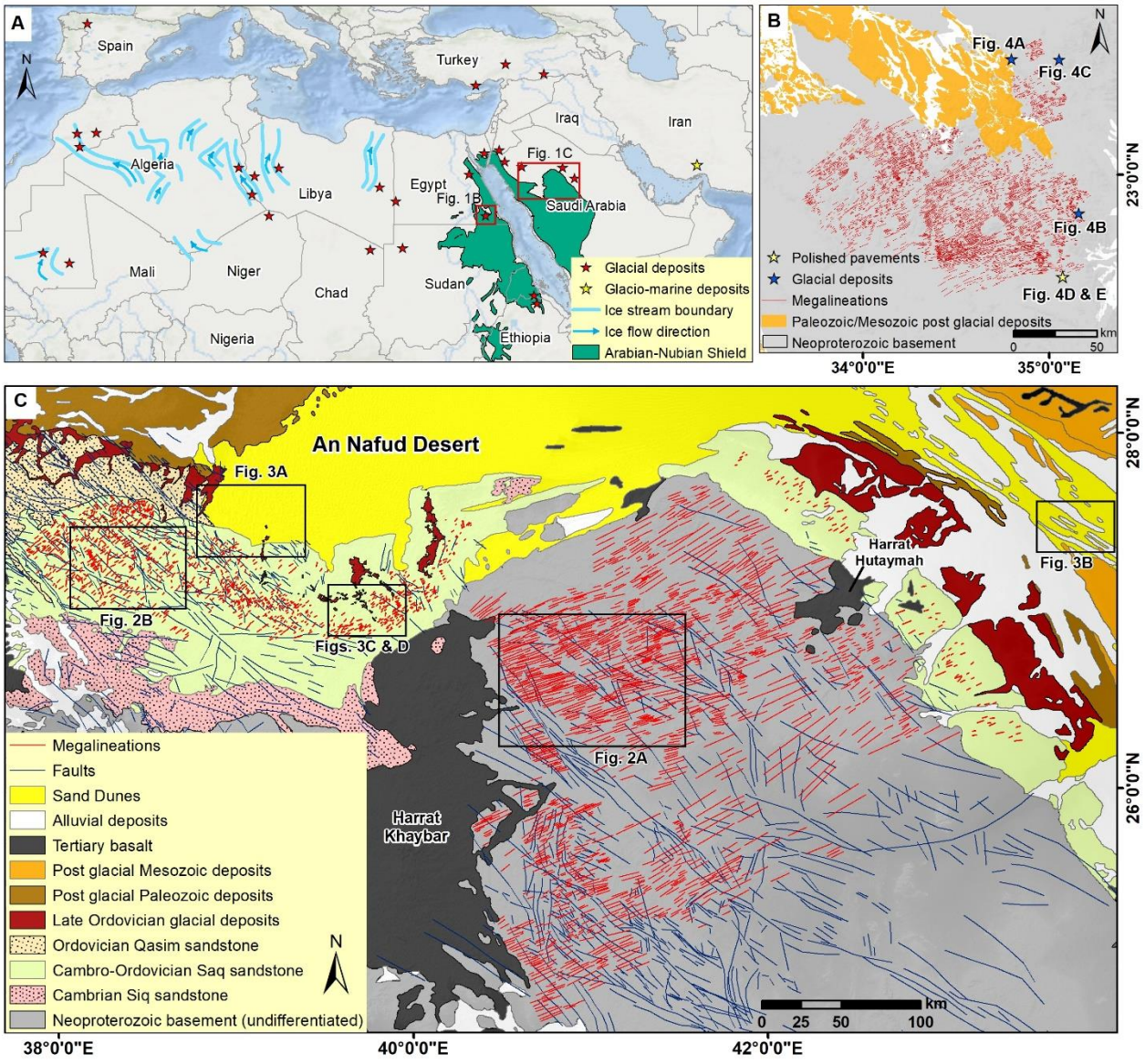

Fig. 1. Location and geologic maps for the Late Ordovician glacial deposits and landforms. (**A**) Location map showing the reported Late Ordovician glacial deposits, landforms, and paleo ice streams [Elhebiry et al.[12]; Le Heron et al.[15]; and references therein]. (**B**) Enlargement of the area covered by the central box in Fig. 1A showing the distribution of MLs and glacial deposits recently mapped in the SED[12]. (**C**) Simplified geologic map for northwest Arabia, showing the difference in the directions of the MLs and the structural trends. Note that the MLs were not

558 reported over the post-Ordovician rock units in southeast Egypt and northwest Arabia. The
559 exhumed MLs extended for 600 km along their strike on both sides of the Red Sea (~200 km in
560 southern Egypt and 400 km in northern Arabia).

561

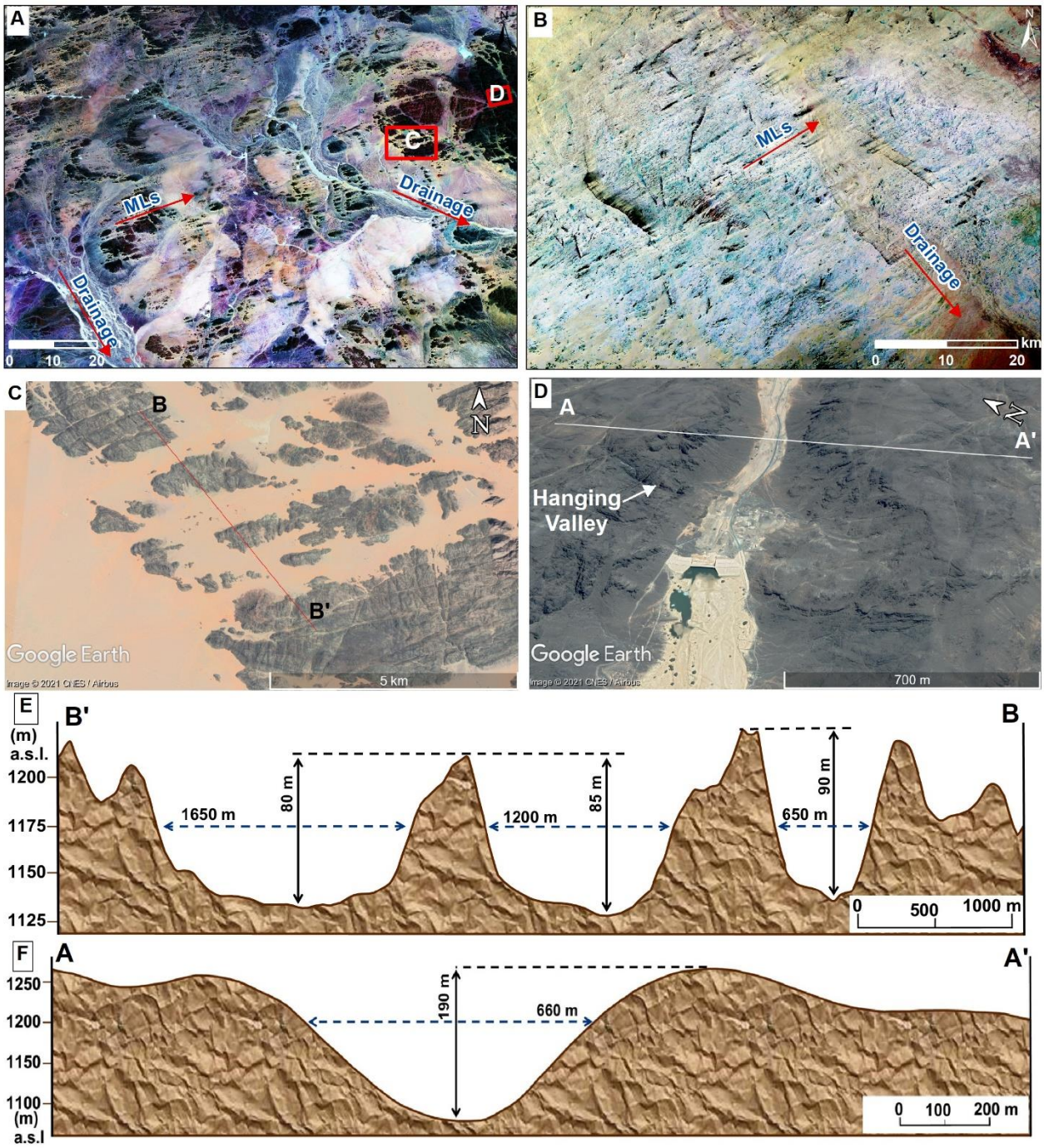

562

563 **Fig. 2. East-northeast–trending streamlined features in northwest Arabia.** (**A**) Landsat 8

564 multi-spectral image (RGB, Landsat; bands 7, 5, and 3) showing the east-northeast–trending

565 MLs over the Cambro-Ordovician Saq Sandstone. (**B**) Landsat 8 multi-spectral image showing

566 the east-northeast trending MLs over the Neoproterozoic basement. (**C**) Google Earth image over

area outlined by box ”C” in Fig. 2A showing sub-parallel ENE-oriented megagrooves incised in a granitic body. (**D**) Google Earth image over area outlined by box “D” on Fig. 2A showing ENE-trending, parabolic U-shaped valley, incised in Neoproterozoic metavolcanics and a N-S-trending hanging valley on its northern side. (**E**) Topographic profile along the cross-section B-B’ in Fig. 2C showing the depth and width of the sub-parallel steep-sided megagrooves (negative topography) separated by megaridges. (**F**) Topographic profile along cross-section A-A’ in Fig. 2D showing the depth and width of the U-shaped valley. Locations of Figs. 2A and 2B are shown in Fig. 1.

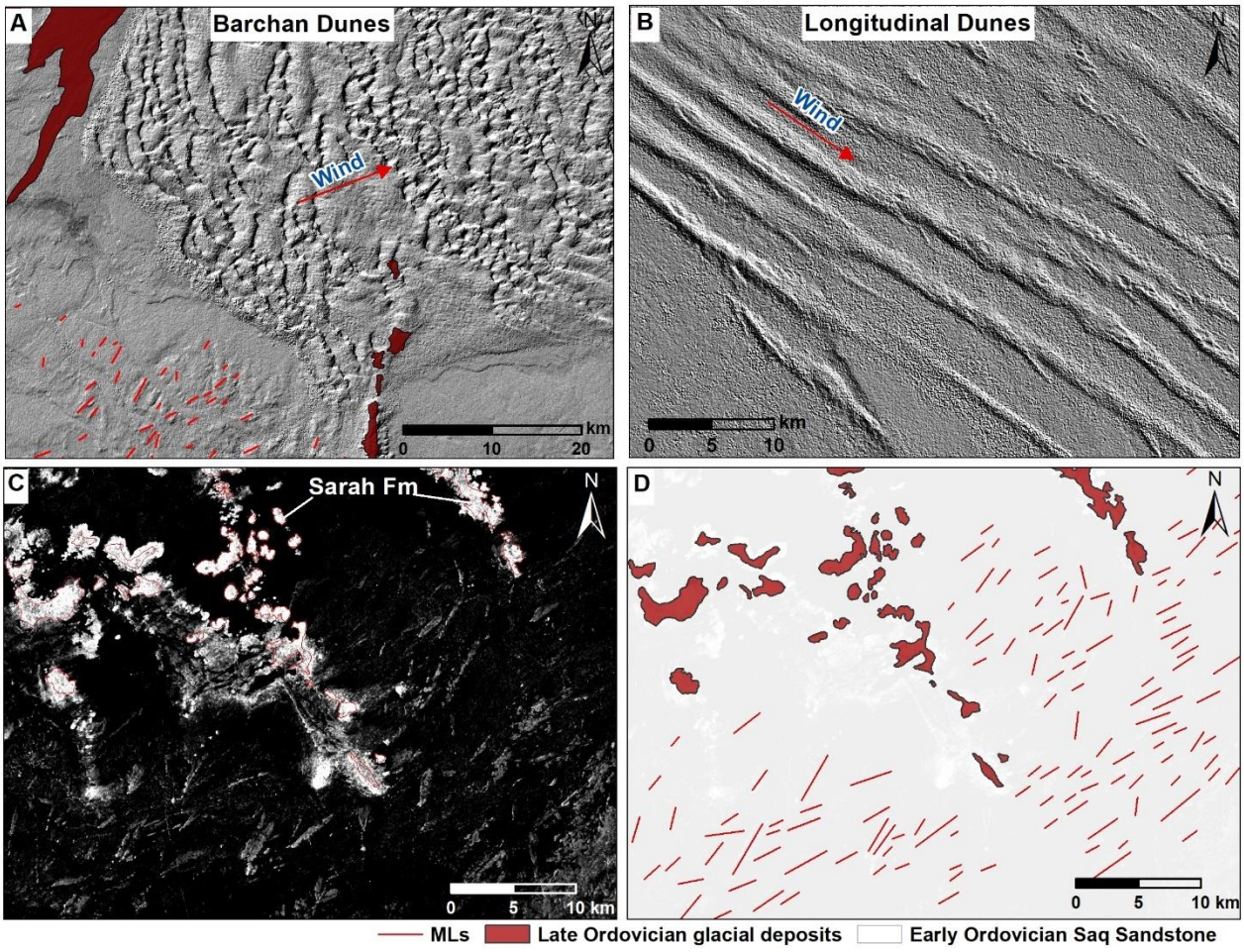

Fig. 3. DEMs and radar images showing the orientation of the MLs, barchan and

578 **longitudinal dunes.** (**A**) SRTM DEM data over the northern part of the study area showing sub-
579 alignment of the streamlined features with the wind direction (southwest to northeast; inferred
580 from the distribution of the barchan dunes in the Nafud dunes). (**B**) ALOS DEM (12.5 m
581 resolution) over the eastern sections of the study area showing wind directions (northwest to
582 southeast; inferred from the longitudinal dune elongation direction) that are at high angles to the
583 MLs trends (east-northeast). (**C**) ALOS PALSAR image showing the Sarah Formation (bright
584 areas outlined by red lines) overlying the MLs; the radar data enables differentiation of linear
585 ridges with rough surfaces (bright, high backscatter) from the valleys floored with fine-grained
586 sand (dark, low backscatter). (**D**) Interpretation map of 2E. Sarah Formation paleo-valleys
587 display inverted topographies[25,46] and are acting as corner reflectors that are characterized by
588 high radar backscatter (bright areas). Locations of Figs. 3A to 3D are shown in Fig. 1C.

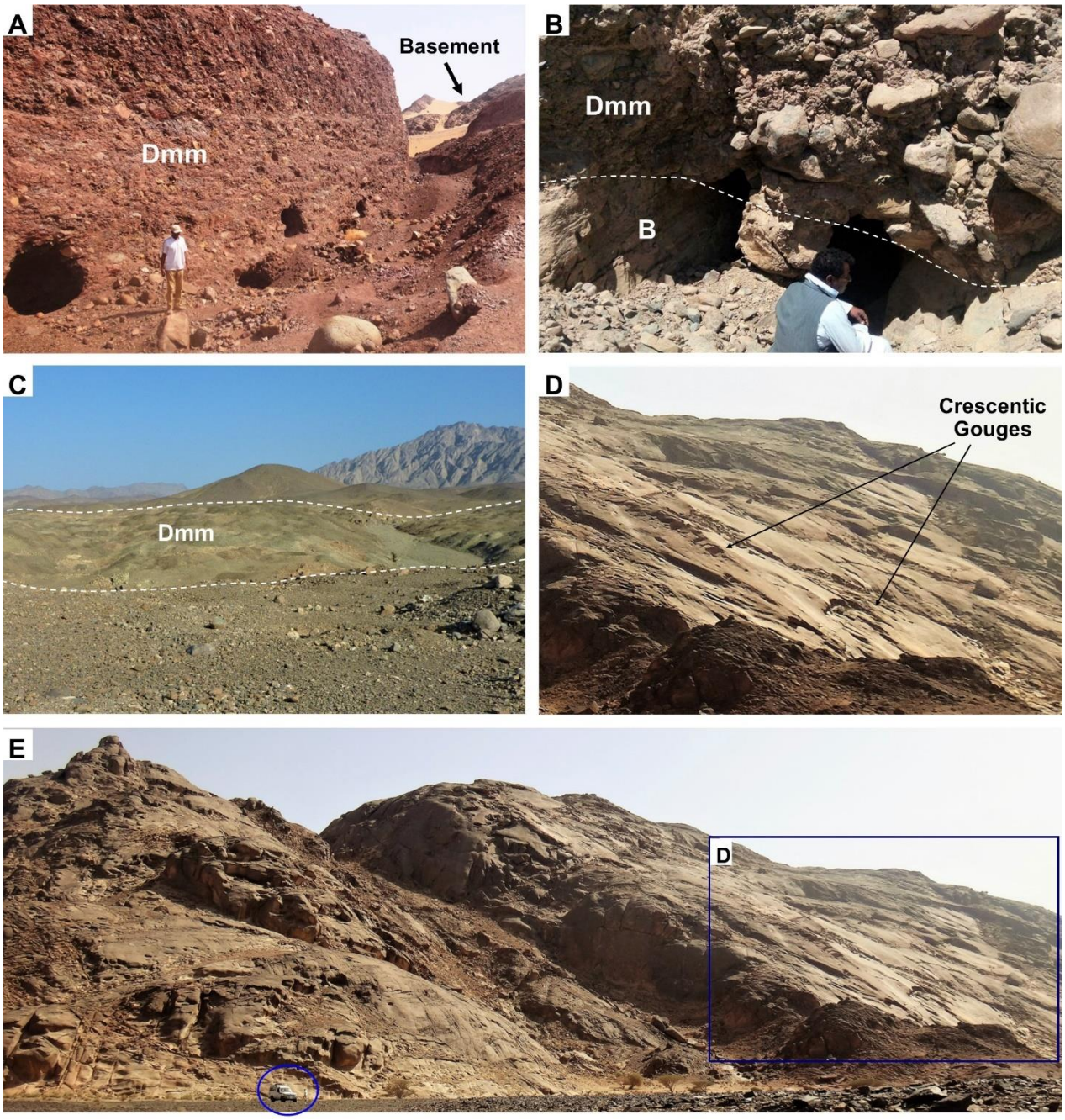

589

590 **Fig. 4. Field photographs for glacial deposits and polished pavements over the**

591 **Neoproterozoic basement of the Arabian-Nubian Shield in the SED of Egypt.** (**A**) Thick

592 glacial deposits (~15m) of massive, unsorted, boulder-rich, and matrix supported diamictites

593 (Dmm) unconformably overlying the basement rocks in Wadi El-Naam area, SED, Egypt. (**B**)

594 Contact between the basement (B) and the overlying unsorted, matrix supported glacial and

595 boulder rich glacial diamictites (Dmm), Korbiai area. (**C**) Glacial diamictites preserved in the
596 paleo-topographic depressions (area ~ 0.5 km^2) within the Neoproterozoic basement in Betan
597 area. (**D**) Enlargement to the area outlined by blue box on Figure 4E, showing glacial polished
598 pavements with crescentic gouges over a Neoproterozoic pluton in the Jebel Hagar Zarqa area.
599 **(E)** Field photograph for the Late Ordovician glacial polished pavements over granitic rocks in
600 the SED. Locations of Figs 4A–4E are shown in Fig. 1B.

601

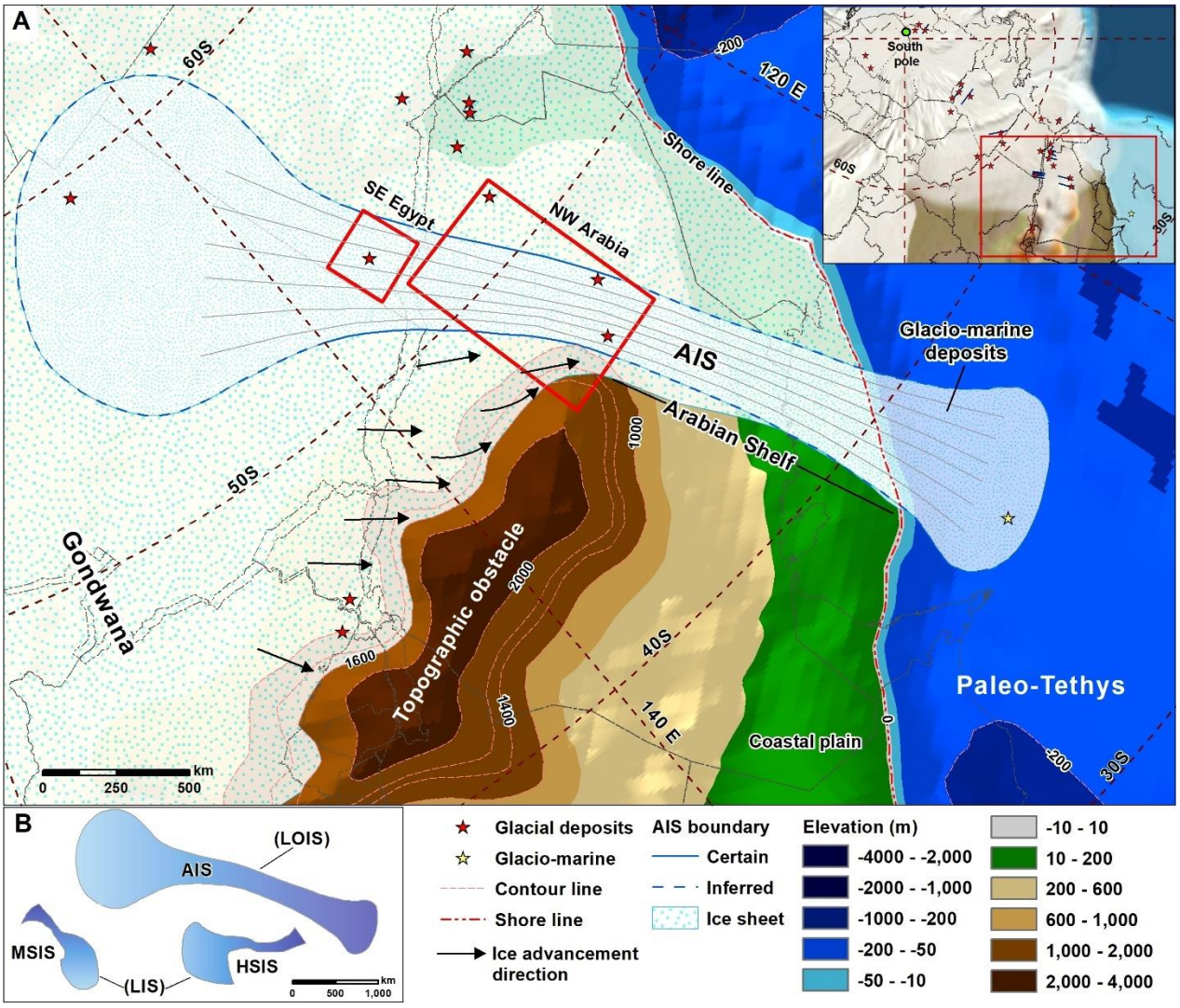

602

603 **Fig. 5. Reconstruction and delineation of the AIS in the Late Ordovician.** (**A**) A detailed

paleo-geomorphological reconstruction for the eastern part of the LOIS and the AIS. All topographic features interpreted from the (1° × 1°) PaleoDEM data[54]. The map indicates the topographic controls for the identified MLs, and the marine terminations of these features. The southern boundary of the AIS was constrained by the location of a topographic high (the Arabian-Nubian shield), whereas the northern margin is not well-defined. Inset map shows paleo-reconstruction for the reported deposits and striation trends from the LOIS plotted over the Gondwana paleo-geographic base map[58]. (**B**) Correlation between the size of the AIS from LOIS and Hudson Strait Ice Stream and M'Clure Strait Ice Stream of the Laurentide Ice Sheet[16], the largest known terrestrial ice streams.

Supplementary Files

This is a list of supplementary files associated with this preprint. Click to download.

- Supplementary1video.mov